Non-autonomy of age-related morphological changes in the *C. elegans* germline stem cell niche

Running title: aging niche morphology

Nilay Gupta[1,2]
Mia Sinks[2]
E. Jane Albert Hubbard[2,3]

[1] Department Biology, New York University
[2] Department of Cell Biology, NYU Grossman School of Medicine
[3] Corresponding author jane.hubbard@nyulangone.org

Keywords: aging, stem cell, DAF-16/FOXO, Insulin/IGF-like signaling (IIS), distal tip cell (DTC), *glp-4*

ABSTRACT

Declines in tissue renewal and repair due to alterations in tissue stem cells is a hallmark of aging. Many stem cell pools are maintained morphologically complex niches. Using the *C. elegans* hermaphrodite germline stem cell system, we analyzed age-related changes in the morphology of the niche, the distal tip cell (DTC), and identified a molecular mechanism that promotes a subset of these changes. We found decreases in the number and length of long DTC processes with age. We also found that a long-lived *daf-2* mutant exhibits a *daf-16*-dependent maintenance of long DTC processes. Surprisingly, the tissue requirement for *daf-16(+)* is non-autonomous, and *daf-16(+)* in body wall muscle is both necessary and sufficient. In addition, after a delay, pre-formed DTC processes deteriorate upon premature germline differentiation, but not upon cell cycle inhibition. We propose a reciprocal DTC-germline interaction model and speculate how reduced *daf-2* activity both delays stem cell exhaustion and maintains DTC processes. These studies establish the *C. elegans* DTC as a powerful *in vivo* model for understanding age-related changes in cellular morphology and their consequences in stem cell systems.

SUMMARY

The *C. elegans* germline stem cell niche morphology is markedly altered with age and is regulated non-autonomously from the muscle by insulin/IGF-like signaling. Results suggest reciprocal niche-germline regulation.

INTRODUCTION

Age-related changes in cell morphology can alter cell-cell interactions and signaling (Lopez-Otin et al., 2023). Such changes are particularly important to understand in stem cell systems where niche cells can take on complex morphologies and associate intimately with the stem cells they regulate (Brunet et al., 2023). Age-related changes in the cytoskeleton, extracellular matrix, cell adhesion properties, and other factors influence cell morphology and function (DiLoreto and Murphy, 2015).

Here, we investigate age-related morphological changes in a simple stem cell niche *in vivo*. Like many mammalian stem cell systems (Brunet et al., 2023; Lopez-Otin et al., 2023), the *C. elegans* hermaphrodite germline stem cell pool becomes depleted with age (Garigan et al., 2002; Killian and Hubbard, 2005; Kocsisova et al., 2019; Luo et al., 2010; Qin and Hubbard, 2015). The niche in this system is a single cell, the distal tip cell (DTC), that caps the end of the gonad (Fig. 1) and produces membrane-bound DSL family ligands, APX-1 and LAG-2, that activate Notch pathway signaling in juxtaposed germline stem cells (Austin and Kimble, 1987; Henderson et al., 1994; Kimble and White, 1981; Nadarajan et al., 2009). The adult DTC morphology is complex, with variable numbers and lengths of long cytoplasmic processes that extend over and between germline stem and progenitor cells (Byrd et al., 2014; Hall et al., 1999; Tolkin et al., 2024). DTC processes are not essential for establishment of the stem cell pool that occurs during larval stages, but they contribute to contact-dependent Notch signaling in adults (Lee et al., 2016).

Here we present an aging time-course analysis of changes in DTC morphology and identify molecular mechanisms that delay or hasten them. Our analysis reveals several striking changes to DTC morphology with age. We confirm an age-related proximal shift in nuclear position that occurs at high penetrance (as seen by others under different life history and age conditions (Kocsisova et al., 2019; Urman et al., 2024)), and that the number and length of long continuous DTC processes decline with age. We examined these phenotypes for their dependence on the DAF-2 insulin-like signaling (IIS) pathway, which influences lifespan. IIS had a relatively minor effect on the nuclear position, but the effects of age on DTC process number and length were highly IIS-dependent. In the *daf-2* mutant, long DTC processes persist with age, and this persistence requires DAF-16/FOXO. Surprisingly, the cellular requirement for *daf-16* is neither the DTC itself, nor does it appear to be the intestine where *daf-16* is implicated in regulating longevity. Instead, *daf-16(+)* activity in the body wall muscle is both necessary and sufficient to regulate age-related changes to the length of the DTC processes. We also

79 determined that pre-formed DTC processes deteriorate prematurely by differentiating the
80 underlying germ line, but not by impeding cell cycle. We propose a reciprocal DTC-germline
81 interaction feedback model whereby DTC processes contribute to stem cell maintenance while
82 stem cells stabilize DTC processes, supporting mutual maintenance in young adults (and in *daf-*
83 *2* mutants) and mutual collapse with age.
84
85
86 **RESULTS**
87
88 ***Adult DTC morphology is altered with age***
89 Age-related changes to hermaphrodite DTC features have been reported previously on a
90 short aging timeline and/or in mated worms (to 5 days of adulthood). These include a proximally
91 displaced nucleus (Kocsisova et al., 2019; Urman et al., 2024) and an increase in the size,
92 though not number, of gaps seen using a membrane reporter (Urman et al., 2024). We sought
93 to further characterize changes to DTC morphology in intact live self-fertile worms over a more
94 extensive timeline from Day 1 to Day 10 of adulthood, and to define morphometric parameters
95 to describe and compare age-related changes under different genetic conditions.
96 To analyze DTC morphology over time, we selected three time points starting from the
97 mid-L4 as determined by vulval morphology (Mok et al., 2015): Day 1 (24 hours post mid-L4),
98 when DTC elaboration has peaked in the wild type; Day 6 post mid-L4, when the reproductive
99 phase of wild-type self-fertile hermaphrodites is ending; and Day 10 post mid-L4, when worms
100 are on the verge of the steep population decline consistent with their ~2-3 week lifespan. To
101 minimize variability due to subtle differences in rearing conditions, for each cohort analyzed,
102 worms were selected as mid-L4 larvae on the same day and harvested for live imaging on Days
103 1, 6, and 10.
104 We examined several different transgenes expressing fluorescent proteins in the DTC,
105 settling on *qIs57* which encodes GFP under the control of the *lag-2* promoter (Siegfried et al.,
106 2004). Compared to the other transgenes we examined, it revealed a suitably detailed set of
107 morphological features, did not appreciably dim with age, and allowed tracking of the position of
108 the nucleus (Fig. S1). To ensure that the transgene was not itself modulating lifespan, we
109 performed lifespan analyses in parallel with the canonical wild-type strain N2 and found no
110 significant difference (Fig. 1A). However, a greater percentage of worms were censored in
111 strains bearing *qIs57* (see Materials and methods). Adult DTCs are morphologically variable;

112 two DTCs from each timepoint are shown in Figure 1B and additional examples are in Figure
113 S2.
114 Using our image analysis pipeline (Gupta et al., 2024), we found several striking
115 changes to DTC morphology with age. Day 1 to Day 10 provides the most informative
116 comparisons (Fig. 1B,C; see Fig. S3 for additional timepoints). First, recapitulating and
117 extending the findings of others (Kocsisova et al., 2019; Urman et al., 2024), we observed that
118 the DTC nucleus, which normally sits at the distal end of the DTC, shifts proximally with age.
119 The percentage of DTCs with the nucleus ≥5 μm from the distal end went from 13% at Day 1 to
120 77% at Day 10, and these nuclei averaged 3 μm and 9 μm from the distal end at Day 1 and Day
121 10, respectively. Second, the number and length of processes extending proximally from the
122 DTC (Byrd et al., 2014; Hall et al., 1999; Tolkin et al., 2024) provided additional parameters that
123 change with age. LAG-2 fusion proteins can be visualized along DTC processes (Henderson et
124 al., 1992; Crittenden et al., 2006; Gordon et al., 2019) and germ cell proximity to processes is
125 associated with higher probability of signal-responding germ cells (Lee et al., 2016). Therefore,
126 changes to DTC processes could conceivably influence the underlying germ cell fate. Though
127 additional parameters may be relevant, we focused on long DTC processes that appeared
128 continuous with the cell body in maximum projection micrographs ("continuous processes"
129 (CPs); Gupta et al., 2024; Tolkin et al., 2024). Our methods do not distinguish between
130 previously-defined subclasses of DTC processes that intercalate with or extend along the germ
131 cells (Byrd et al., 2014), but they reflect only gross morphological features including the
132 proportion of DTCs with processes that extend beyond a 20 μm threshold from the distal end,
133 and the numbers and lengths (mean and maximum) of such processes. At Day 1 post mid-L4,
134 all DTCs had at least one process extending beyond 20 μm. By Day 10, 14% of DTCs had no
135 CPs beyond this threshold. Among those DTCs with one or more CP over the threshold, we
136 observed fewer and shorter CPs over time: the mean number of CPs decreased from 11 to 4
137 from Day 1 to Day 10, as did their mean and maximum lengths (mean 37 to 30 μm, and
138 maximum 60 to 38 μm) (Fig. 1C).
139
140 ***Insulin/insulin-like growth factor-1 signaling (IIS) promotes age-related changes in DTC***
141 ***process number and length***
142 The IIS pathway is highly conserved and modulates longevity in *C. elegans*, *Drosophila*,
143 and mice (Kenyon, 2010b; Murphy and Hu, 2013; Russell and Kahn, 2007). In addition to
144 longevity, IIS regulates various physiological processes in *C. elegans*, including development,
145 metabolism, and stress resistance (Murphy and Hu, 2013). DAF-2 is the sole insulin/IGF-1

146 receptor in *C. elegans* (Kimura et al., 1997), and reducing *daf-2* activity (e.g. by the reduction-of-
147 function *(rf) daf-2(e1370)* allele) extends lifespan (Kenyon et al., 1993). To determine whether a
148 reduction in *daf-2* activity would affect age-related changes in DTC morphology, we examined
149 DTCs in *daf-2(rf)* worms. First, we tested whether the *qIs57* marker affected the *daf-2(rf)*
150 longevity phenotype and found that, if anything, the percentage of worms alive between 40-60
151 days was elevated, but the maximum lifespan was similar (Fig. 1A). We aged cohorts of wild-
152 type and *daf-2(rf)* worms in parallel and measured the parameters as described above.
153 First, we found that *daf-2(rf)* had a minimal and variable effect on age-related nuclear
154 position displacement (Figs 1C, S3A). Relative to the wild type, *daf-2(rf)* displayed a reduced
155 proportion of DTCs that exhibit nuclear displacement of ≥5 μm at Day 10. However, a large
156 percentage (47%) of *daf-2(rf)* worms nevertheless displayed the nuclear displacement
157 phenotype (versus 77% in the wild type), and the average degree of displacement in microns
158 from the distal end was similar to the wild type in this cohort. The latter finding is consistent with
159 those of Kocsisova et al. (Kocsisova et al., 2025, their Fig. S1). In summary, nuclear
160 displacement occurs at a high penetrance in both wild type and *daf-2(rf)* with an equal distance
161 of displacement, suggesting that IIS plays a minor role in regulating this aspect of age-related
162 changes to DTC morphology.
163 In contrast to the minor effects on nuclear position, reducing *daf-2* activity virtually halted
164 age-related changes in CP number and length from Day 1 to Day 10: all *daf-2(rf)* worms
165 possessed at least one CP ≥20 μm at Day 10, and there was no decrease in the average
166 number of CPs ≥20 μm, nor their mean or maximum lengths, as was seen in the wild type (Figs
167 1C, S4). We therefore focused on the DTC phenotypes related to number and length of CPs.
168
169 ***The persistence of DTC process number and length in daf-2(rf) does not correlate***
170 ***temporally with extended lifespan or reproductive span***
171 In addition to lifespan extension in *daf-2(rf)*, the reproductive span of self-fertile
172 hermaphrodites averages several days longer (Dillin et al., 2002), and in mated hermaphrodites,
173 the *e1370* allele, in particular, delays reproductive aging (Kocsisova et al., 2025). We wondered
174 whether the rate of age-related changes in the number and length of DTC processes might
175 correlate with reproductive span and/or population lifespan. If correlated with reproductive span,
176 we would expect DTC processes to be shorter after a week in *daf-2(rf)*. If the rate of decline
177 were associated with average lifespan, we would expect to observe shorter processes by 30
178 days. We therefore collected additional measurements in *daf-2(rf)* up to Day 30 (Fig. 1D;
179 additional timepoints in Fig. S3B). Referencing our lifespan measurements, Day 30 in *daf-2(rf)*

180 reflects the percent alive of wild type at Day 15. We found that, remarkably, while the number of
181 CPs declined modestly in this cohort by Day 30 (Fig. 1D), it still remained above that of the wild
182 type at Day 10 (Fig. 1C). In addition, there was no statistically significant decline in the mean
183 length of CPs ≥20 μm up to 30 days. Although we observed a significant decline in the
184 maximum length, the average is still longer than the wild type at Day 10.
185 We conclude that reducing *daf-2* markedly delays age-related changes in the number
186 and length of long DTC processes, and that these changes in DTC morphology do not directly
187 correlate with temporal extension of reproductive span or of population lifespan.
188
189 ***Insulin/insulin-like growth factor-1 signaling (IIS) acts via DAF-16/FOXO to promote age-***
190 ***related changes in DTC process length***
191 Many phenotypes of *daf-2(rf)* mutants, including age-related phenotypes such as
192 lifespan, depend on the DAF-16/FOXO transcription factor (Kenyon, 2010a; Murphy and Hu,
193 2013).To determine whether the *daf-2*-dependent age-related changes in DTC process number
194 and length are also dependent on *daf-16*, we examined DTC morphology, as visualized with the
195 *qIs57* marker, in double mutant strains bearing a *daf-16* null mutation *daf-16(mu86)* and *daf-*
196 *2(e1370)* [hereafter referred to as *daf-16(0); daf-2(rf)*]. Although the vast majority of DTCs had
197 one or more CP that exceeded 20 μm, the number of processes and their mean and maximum
198 length decreased similar to the wild type (Fig. 2).
199 To assess the loss of *daf-16* alone, we measured the same parameters in parallel
200 cohorts with the wild type, *daf-2(rf)*, and *daf-16(0); daf-2(rf)* (Figs 2, S5). In these trials, a small
201 percentage of CPs of Day 10 DTCs in *daf-16(0)* worms did not exceed 20 μm, though not as
202 many as the wild type. CP number and length also decreased, as in the wild type. Taken
203 together, we conclude that the maintenance of DTC process number and length over time in
204 *daf-2(rf)* is highly dependent on *daf-16* activity.
205
206 ***Non-autonomous daf-16 activity influences age-related decline of DTC process length***
207 Prior studies indicated that *daf-16* activity in specific tissues can influence distinct
208 phenotypes while also contributing to systemic effects. For example, intestinal *daf-16* is
209 associated with enhanced stress resistance and increased longevity (Libina et al., 2003; Zhang
210 et al., 2022), and *daf-16* in the germ line and muscle promotes expansion of the progenitor pool
211 during germline development (Michaelson et al., 2010). Additionally, *daf-16* activity in *fos-1a*
212 expressing cells in the proximal somatic gonad (PSG) prevents the age-dependent decline in
213 number of germline progenitors (Qin and Hubbard, 2015). Therefore, we sought to determine in

214 which tissues *daf-16* most influences the maintenance of DTC processes with age that we
215 observed in *daf-2(rf)*. For this analysis, we focused on the DTC length parameters (mean and
216 maximum).
217 Our first approach took advantage of available extrachromosomal arrays (Libina et al.,
218 2003; Qin and Hubbard, 2015). Each includes a tissue-restricted promoter driving a GFP::DAF-
219 16a translational fusion. We performed the aging time course in the *daf-16(0); daf-2(rf)*
220 background and compared DTC processes length parameters from control and array-bearing
221 (phenotypically Rol) worms, and non-array bearing (phenotypically non-Rol) progeny from the
222 same array-bearing mothers. If *daf-16(+)* activity were important in a particular tissue location,
223 we expected that its expression would preserve DTC process length relative to *daf-16(0); daf-*
224 *2(rf)*.
225 To assess the approach, we first examined CPs in worms bearing an array that
226 expresses *daf-16a* from the *daf-16* promoter. We observed that these parameters (the
227 proportion of worms with DTC CPs over 20 μm, and the CP length – both mean and maximum)
228 were markedly stable relative to *daf-16(0); daf-2(rf)* (Fig. 3) and to non-array bearing siblings
229 (Fig. S6). The phenotypic similarity of *daf-16(0); daf-2(rf)* to non-array bearing progeny from
230 array-bearing mothers also suggested that the array did not confer a maternal effect.
231 We next tested for DTC-autonomy, expressing *daf-16a* from the *lag-2* promoter
232 (Michaelson et al., 2010). Surprisingly, ~15% of ~140 DTCs exhibited an unusual morphology at
233 Days 6 and 10, half displaying uncharacteristically long DTC processes, while others displayed
234 one thick CP containing a displaced nucleus (Fig. S7). None of these features were observed
235 under any other condition. Among the remaining ~85% of DTCs that exhibited normal
236 morphology, the CP length parameters were similar to *daf-16(0); daf-2(rf),* even though ~10% of
237 the DTCs in array-bearing worms at Day 10 had no CPs ≥ 20 μm (Figs 3, S6). Thus, apart from
238 the low-penetrance alterations in gross morphology, *lag-2*-driven *daf-16a(+)* had no appreciable
239 effect on the persistence of DTC process length with age. We conclude that non-autonomous
240 *daf-16a(+)* activity is sufficient to prevent the age-related decline in DTC length when *daf-2* is
241 reduced.
242
243 ***Intestinal activity of daf-16a does not appear to promote age-related DTC length in daf-***
244 ***2(rf)***
245 Both heterologous expression approaches (Libina et al., 2003) and protein degradation
246 approaches (Zhang et al., 2022) indicate that the intestine is the major contributor of *daf-16*
247 activity that confers extended lifespan in *daf-2(rf)*. We speculated that changes in DTC

morphology might be a function of overall organismal aging. If so, we would expect that intestinal *daf-16(+)* in the *daf-16(0); daf-2(rf)* mutant background would stabilize DTC processes, similar to *daf-16(+)* driven by its own promoter.

Again, using the same transgene expressing *daf-16(+)* that alters lifespan (Libina et al., 2003), we tested the sufficiency of *daf-16a* expressed from an intestine-specific promoter. We found that although all worms bore DTCs with CPs ≥ 20 μm, CP lengths still declined significantly with age, comparable to that observed in *daf-16(0); daf-2(rf)* controls (Figs 3, S6). In conclusion, although intestinal *daf-16(+)* contributes the majority of the longevity phenotype in *daf-2(rf)* (Libina et al., 2003; Zhang et al., 2022), it does not appear to regulate the length of DTC processes with age.

Neuronal daf-16a(+) activity mildly influences the age-related changes in DTC length

Although the intestine is the major contributor of *daf-16* on lifespan, there is neuronal contribution as well (Uno et al., 2021; Zhang et al., 2022). We tested an array expressing *daf-16a(+)* from a pan-neuronal promoter and observed that while all DTCs in the worms bearing the neuronally-expressed *daf-16a(+)* array contained CPs that crossed the 20 μm threshold, the CPs showed a modest but significant length decline with age. We conclude that neuronal activity of *daf-16(+)* makes a minor contribution to maintaining the length of DTC processes with age in *daf-2(rf)*.

Proximal somatic gonad (PSG) daf-16a(+) activity does not prevent the age-related loss of DTC process length

Previous results indicate that *daf-16a* expressed in *fos-1a*-positive cells of the proximal somatic gonad (PSG) in a *daf-16(0); daf-2(rf)* double mutant delays age-dependent loss of germline progenitors (Qin and Hubbard, 2015), and *daf-16*-dependent DOS-3, a non-canonical ligand for the GLP-1/Notch receptor, is a relevant PSG signal (Zhang et al., 2024). We hypothesized the PSG-expressed *daf-16* might also contribute to DTC morphology. Although prior experiments used *naEx239[*pGC629*(fos1p::gfp::daf-16a)* + pRF4*]* in *daf-16(m26); daf-2(e1370)* (Qin and Hubbard, 2015), for consistency between experiments here, we moved the array into the *daf-16(mu86); daf-2(rf)* background, and measured CP number and length.

In short, *daf-16a(+)* activity in the PSG did not prevent the age-dependent loss of DTC process length. However, these worms were markedly less healthy than other strains bearing *daf-16(+)* arrays: only ~50% of worms survived to Day 4, a defect not observed with other *daf-16(+)* arrays. Moreover, nearly a third (29%) of worms bearing the array had no DTC process

282 ≥20 μm. Of those that did, the mean and maximum lengths were lower than the control on Day
283 1 and nevertheless continued to decrease with age (Figs 3A, S6).
284 Collectively, these findings demonstrate that the expression of *daf-16a(+)* via *fos-1a*
285 promoter is insufficient to prevent the age-dependent DTC process decline in a *daf-16(0); daf-*
286 *2(rf)* background. This result raises the possibility that while *daf-16a(+)* in the PSG promotes
287 maintenance of the progenitor pool with age (Qin and Hubbard, 2015; Zhang et al., 2024), it
288 does not delay the decline of DTC process length with age.
289
290 ***Germline daf-16 exerts a minor effect on DTC process length***
291 The germ line is the major focus of activity for *daf-16* in modulating expansion of the
292 progenitor zone (PZ) in larval stages (Michaelson et al., 2010), and the development of adult
293 DTC morphology is partially dependent on the germ line (Tolkin et al., 2024). To determine
294 whether germline *daf-16* is required for long continuous DTC processes to persist in *daf-2(rf)*,
295 we used RNAi feeding and the *rrf-1* mutant in which RNAi is less effective in the soma but is
296 retained in the germ line (Kumsta and Hansen, 2012; Sijen et al., 2001). We note that in these
297 experiments (as in Fig. 2) *daf-2(rf)* displays an increase in mean (Fig. 3B) and maximum (Fig.
298 S8) CP length from Day 1 to Day 10, an effect that is not observed with *rrf-1* alone (Fig. S8).
299 We speculate that this may be related to a delay in the PZ reaching its maximum size in *daf-*
300 *2(rf)* worms (see Discussion). As expected from the foregoing mutant analysis, reducing *daf-16*
301 by RNAi eliminated the mean and maximum CP length increase observed in *daf-2(rf)* from Day
302 1 to Day 10. In the absence of *rrf-1*, however, the mean CP length increased in both the L4440
303 control and with *daf-16(RNAi)*, suggesting that the contribution of *daf-16* from the soma is more
304 relevant for mean CP length. For maximum length (Fig. S8), a minor effect of *daf-16(RNAi)* is
305 seen in the absence of *rrf-1*. We conclude that germline *daf-16* plays a minor to negligible role in
306 regulating DTC processes in *daf-2(rf)* with age.
307
308 ***Body wall muscle-specific daf-16a(+) is sufficient and necessary for the DTC process***
309 ***length reduction with age in daf-2(rf)***
310 We measured DTC parameters in *daf-16(0); daf-2(rf)* worms bearing an array
311 expressing *daf-16a(+)* in body wall muscle (*myo-3p::GFP::daf-16a*; Libina et al., 2003). All the
312 worms carrying the array had CPs ≥20 μm (Fig. 3A). Furthermore, CP length was maintained in
313 *daf-16(0); daf-2(rf)* relative to controls without the array and was similar to worms carrying the
314 *daf-16p::daf-16(+)* array (Figs 3A, S6). We also did not observe a significant effect of muscle
315 *daf-16(+)* on the extension of reproductive span that is seen in *daf-2(rf)* alone nor an increase in

316 self-fertile brood size (Fig. S9A). Together, these findings indicate that array-borne expression
317 of *daf-16a* in body wall muscle is sufficient to maintain the length of DTC processes with age in
318 *daf-2(rf)*.
319 To assess the necessity of body wall muscle DAF-16, we used an auxin-mediated
320 degron approach (Zhang et al., 2015). We generated a strain bearing *daf-2(rf),* a *TIR1::mRub*y
321 fusion expressed under the *myo-3* promoter (Sabatella et al., 2021) together with degron-tagged
322 DAF-16::GFP (Zhang et al., 2022), and the DTC marker. Following the red and green
323 fluorescent protein tags, we confirmed the tissue-specific expression of TIR1 and auxin-
324 dependent loss of DAF-16 (Fig. S10A). In all of the vehicle controls (*daf-2(rf)* and the DAF-
325 16::degron alone), the DTCs in *daf-2(rf)* strains not only maintained but increased in length over
326 the 10 day interval, while mean length of DTC processes in the strain bearing both *myo-*
327 *3p::TIR1* and the degron-tagged DAF-16 decreased (Figs 3C, S6). Although DAF-16::GFP was
328 undetectable with auxin exposure, the relatively modest effect could be due to residual
329 undetectable DAF-16.
330 These results suggest that *daf-16* in body wall muscle is a major contributor to the
331 persistence of long DTC processes in *daf-2(rf)* with age.
332
333 ***Body wall muscle DAF-16a attenuates the rate of germline progenitor zone decline with***
334 ***age***
335 Prior studies implicated muscle-expressed *daf-16a* activity in a minor but significant role
336 downstream of *daf-2* in promoting larval expansion of the germline progenitor pool (Michaelson
337 et al., 2010), whereas it did not significantly influence the endpoint of the progenitor cell number
338 in aged worms (Qin and Hubbard, 2015).
339 Our DTC morphology analysis prompted us to re-examine the possibility of a role for
340 *myo-3p::daf-16a(+)* in maintaining the PZ pool over an aging time-course in *daf-2(rf)*. We found
341 that the PZ pool of *daf-16(0); daf-2(rf)* worms expressing *myo-3p::daf-16a(+)* started with fewer
342 cells than *daf-16(0); daf-2(rf)* on Day 1, consistent with the results of Michaelson et al. (2010).
343 Relative to controls, *daf-16(0); daf-2(rf)* with *myo-3p::daf-16a(+)* also does not affect the
344 terminal PZ cell count, consistent with the results of Qin and Hubbard (2015). However, the
345 presence of the *myo-3p::daf-16a(+)* array does attenuate the rate of decline of the PZ, similar to
346 *daf-2(rf)* (Figs 4A, S9B). This result suggests that the slower PZ loss over time in *daf-2(rf)* is
347 partially dependent on muscle-produced *daf-16(+)*. Other tissues likely contribute, since an
348 array bearing *daf-16(+)* driven from its own promoter gives a stronger effect. By contrast,

349 muscle-produced *daf-16(+)* prevents loss of DTC processes length over time, similar to what is
350 observed with *daf-16(+)* driven by its own promoter.
351 We further asked whether altering *daf-2* and *daf-16,* and in particular *daf-16a(+)* from
352 muscle, would influence the proportion of gonads displaying active cell divisions (mitotic figures)
353 on Day 10, a time-point at which we observed no mitotic figures in the wild type. We found
354 significantly more *daf-2(rf)* worms display mitotic figures at Day 10, while *daf-16(0); daf-2(rf)* do
355 not, though the *daf-16(0); daf-2(rf)* proportion is intermediate, suggesting that only part of this
356 phenotype may be *daf-16*-dependent. Of *daf-16(0); daf-2(rf)* worms expressing *myo-3p::daf-*
357 *16a(+)*, 28% display mitotic figures, similar to worms expressing *daf-16p::daf-16a(+)*. These
358 results suggest that muscle-expressed *daf-16a(+)* could play a role in maintaining Day 10 germ
359 cell cycling in self-fertile *daf-2(rf)* hermaphrodites. Overall, muscle-expressed *daf-16(+)* both
360 delays age-related changes to the PZ pool and to the DTC, with more subtle effects on the PZ
361 than the DTC, though other tissues also contribute to each independently (see Discussion).
362
363 ***Germline undifferentiated fate status, but not cell cycle progression, is correlated with***
364 ***maintenance of DTC processes***
365 A striking feature of the aged *daf-2(rf)* germ line is the relative stability of the PZ pool
366 compared to the wild type (Figs 4A, S9B). In mated worms, *daf-2(rf)* also displays a more
367 proximal border of SYGL-1-positive stem cells and a more constant position of meiotic entry
368 relative to the wild type (Kocsisova et al., 2025). We further observed that the proportion of
369 gonads with active divisions in Day 10 is higher in *daf-2(rf)* and the mitotic index did not decline
370 significantly from Day 1 to Day 10, and that all these phenotypes are partially dependent on *daf-*
371 *16* (Figs 4A-B, S9B-C). These results prompted us to consider the relationship between DTC
372 processes, stem cell fate, and mitotic progression.
373 Out-growth of the DTC processes in early adulthood is dependent on an underlying
374 substrate of the undifferentiated germ cells (Byrd et al., 2014; Tolkin et al., 2024). We therefore
375 wondered whether adult DTC processes, once formed, would be stable in the absence of the
376 underlying PZ in early adulthood. We analyzed the number and length of long DTC processes in
377 worms bearing a temperature sensitive allele of *glp-1/* Notch, *glp-1(e2141),* in which the entire
378 PZ differentiates at the restrictive temperature (Austin and Kimble, 1987). We examined the
379 nuclear morphology of distal germ cells and measured DTC parameters from parallel cohorts of
380 worms that underwent the same temperature-shift regime (Fig. 5A). After 24 hours at the
381 restrictive temperature, although virtually all distal germ cells had entered meiotic prophase, the
382 CP number and length parameters were unaffected (Fig. S11A-C). By 48 hours, however, the

383 CP length was reduced relative to the wild type (Fig. 5A-C). We conclude that premature
384 differentiation of the PZ pool causes a premature decline in the complexity of the DTC
385 morphology, but with a time delay between differentiation and the decline of DTC processes.
386 Because differentiated germ cells no longer divide, and because *daf-2(rf)* display more
387 mitotic figures than the wild type at a late time point (Day 10; Figs 4B, S9C), and this phenotype
388 is partially dependent on muscle-expressed *daf-16(+)*, we wondered whether the DTC process
389 maintenance requires active cycling in the underlying germline stem/progenitor cells. To test this
390 possibility, we used a temperature sensitive allele of *glp-4, glp-4(bn2),* that causes germ cell
391 cycle arrest in pro-metaphase; arrested *glp-4* germ cells are resistant to differentiation, even in
392 the absence of *glp-1* (Beanan and Strome, 1992). Remarkably, after 48 hours at the restrictive
393 temperature, although *glp-4* mutant gonads display altered nuclear morphology, the DTC
394 processes did not collapse (Figs 5D-F, S12A-C). We further observed that germ cells were
395 capable of recovery after shifting back to the permissive temperature for another 48 hours, and
396 the DTC processes remained intact (Fig S12A-C).
397 Therefore, while loss of stem cells to differentiation eventually leads to changes in DTC
398 morphology that resemble what is seen in older adults, interfering with cell cycle without causing
399 differentiation (as in *glp-4* at the restrictive temperature) does not.
400
401 **DISCUSSION**
402
403 Here we define age-related changes in DTC niche morphology and assess their
404 dependence on IIS, a molecular mechanism that affects longevity. We found that an age-related
405 shift in DTC nucleus position is only modestly affected by IIS in self-fertile hermaphrodites, as
406 was previously shown in mated worms (Kocsisova et al., 2019), while the decline in the number
407 and length of long DTC processes is highly dependent on IIS. We identify body wall muscle as a
408 major source of a *daf-16(+)*-dependent activity that can support both the persistence of long
409 DTC processes in a *daf-2(rf)* mutant and the underlying germline progenitor pool. Finally, we
410 determine a dependency relationship between the germ cell proliferative state and maintenance
411 of pre-formed DTC processes.
412
413 ***A model for reciprocal feedback interactions between the aging germline and niche***
414 In a seeming paradox, *daf-2(+)* expands the larval germline progenitor zone (PZ) but
415 drives loss of the PZ with age, and both effects are dependent on *daf-16*. In larvae, the germline
416 cell cycle is slower in worms with reduced *daf-2* activity and this is dependent on *daf-16(+)* in

417 the germ line and body wall muscle (Michaelson et al., 2010; Roy et al., 2016). In aged adult
418 worms, a larger PZ pool is maintained with reduced *daf-2* activity (Qin and Hubbard, 2015; Fig.
419 4A). In this case, one *daf-16*-dependent signal, DOS-3, from the proximal somatic gonad likely
420 supports GLP-1/Notch activity in the germ line (Zhang et al., 2024). We found that, in addition,
421 both the PZ pool and long DTC processes are maintained in old *daf-2(rf)* adults in a *daf-16(+)*
422 muscle-autonomous manner. The exact *daf-16*-dependent mechanism – and whether it acts on
423 the directly on the DTC, the germline, or both – awaits further study. We speculate that such a
424 factor could be a *daf-16*-dependent secreted factor – e.g., a mitokine or myokine signaling
425 mechanism, or some other mechanism secondary to the IIS role in muscle function (Herndon et
426 al., 2002; Wang et al., 2019). There is precedent for body wall muscle-produced secreted
427 proteins acting on the germ line, including HIM-4/hemicentin (Vogel and Hedgecock, 2001) and
428 SWM-1 (Chavez et al., 2018).

429 Regardless of the exact mechanism, these observations suggest a model for interplay
430 between the control of cell fate and cell cycle rate that may contribute to the dynamics of the
431 germline stem cell system over time with age. Several additional relevant features of the system
432 are noted below.

433 First, stem cell fate and cell cycle rate are independently controlled. The PZ consists of a
434 distal-most SYGL-1(+) germline stem cells (GSCs) that are actively responding to GLP-1/Notch
435 (Kershner et al., 2013), as well as their more proximal SYGL-1(-) progeny that complete a cell
436 division before differentiating (Fox and Schedl, 2015). Reducing *glp-1* activity moves the border
437 of the PZ distally and reduces the number of GSCs but, importantly, does not alter their rate of
438 cell cycle progression (Fox and Schedl, 2015; Michaelson et al., 2010; Roy et al., 2016). By
439 contrast, reducing *daf-2* slows the cell cycle (e.g., lowers M-phase and S-phase indices, a rough
440 proxy) in larvae but does not influence the stem versus non-stem cell fate decision governed by
441 GLP-1/Notch (Michaelson et al., 2010; Roy et al., 2016). Worms with reduced *daf-2* activity
442 therefore reach adulthood with fewer cells PZ cells. This pool declines with age, but at a rate far
443 slower than the wild type (Kocsisova et al., 2022; Qin and Hubbard, 2015; Fig. 4A). Second, as
444 in many mammalian stem cell systems (Brunet et al., 2023), *C. elegans* GSCs become depleted
445 over time (Kocsisova et al., 2019; Qin and Hubbard, 2015), and, importantly, the PZ pool is
446 effectively "used up" with age. This loss is accelerated in the presence of replete sperm that
447 encourage germline flux (Kocsisova et al., 2019; Qin and Hubbard, 2015). In addition, with age,
448 the mitotic index slows, even in the presence of replete sperm (Kocsisova et al., 2019). Finally,
449 in early adulthood, the outgrowth of DTC processes partially depends on adhesion to underlying
450 proliferative germ cells (Tolkin et al., 2024).

451 Taking these observations together, we propose a two-component feedback system that
452 supports homeostasis of the progenitor pool in early adulthood, and the loss of which
453 contributes to the collapse of both niche morphology and the stem cell pool with age. In this
454 model, the early adult PZ steady state is maintained by a combination of DTC-to-GSC signaling
455 via GLP-1/Notch to designate the stem cell fate in responding germ cells, as well as DAF-2-
456 dependent inputs that promote continued stability of DTC processes. Over time, however, as
457 cells leave the PZ through differentiation (meiotic entry) and the pool of undifferentiated germ
458 cells becomes depleted, overlying DTC processes are not maintained due to both loss of DAF-
459 16-dependent muscle (and other) effects, as well as PZ depletion. Decreased ligand availability
460 due to shortened DTC processes would then further deplete the stem cell pool and further
461 destabilize the DTC processes.

462 In the *daf-2(rf)* scenario, we propose that in addition to the effect on *daf-16*, the
463 persistence of slow-cycling yet undifferentiated germline stem/progenitor cells may contribute to
464 the stability of DTC processes, perhaps by adhesion mechanisms similar to those that act in the
465 early adult (Tolkin et al., 2024). This stability could then support DTC-to-GSC interactions along
466 the DTC processes that help maintain stem cell fate (Fig. 5D). Again, GLP-1/Notch signaling
467 afforded by stable DTC processes may, in turn, support germ cells in an undifferentiated,
468 proliferation-competent (and continued slow-cycling) state. Reducing *daf-2* would thereby delay
469 the age-related declines in both components of the reciprocal interaction that are mutually
470 supportive, the progenitor pool and niche morphology.

471 Temporally, the decline of the stem cell pool and PZ precedes that of the DTC
472 processes (Figs 1, 4). Similarly, when germ cells are forced to differentiate, a time delay occurs
473 before the DTC declines (Fig. 5). We observed that loss of *glp-1*, which causes germ cells in the
474 PZ to differentiate, leads to premature collapse of already-formed DTC processes while loss of
475 *glp-4*, which impedes the cell cycle but does not cause differentiation does not cause the
476 collapse of DTC processes. These results implicate the undifferentiated state of germ cells in
477 the germline-to-DTC branch of the feedback to help maintain DTC processes.

478 While this model provides a framework for reciprocal signaling between DTC processes
479 and the germ line, additional influences act on the system. For example, the regulation of GLP-
480 1/Notch signaling with age (Kocsisova et al., 2019) is complex: in addition to DOS-3-mediated
481 signaling from the proximal somatic gonad (Zhang et al., 2024), the shift in the position of the
482 DTC nucleus also alters the patterning of signaling (Urman et al., 2024), and there may be
483 germline-autonomous aspects of reduced GLP-1/Notch signaling since, at least to Day 4, *sygl-1*
484 RNA levels do not change (Urman et al., 2024). In mated worms, reduced Notch signaling is

485 implicated in depletion of the stem cell pool and reproductive aging, both of which are also
486 delayed in mated *daf-2(rf)* worms (Kocsisova et al., 2025). It will be of interest to determine,
487 ideally in individual gonads, to what extent reduced ligand signaling due to changes in DTC
488 morphology with age contribute to the age-related decline in the germline stem cell pool and
489 subsequent reproductive aging.
490 Our model also predicts that the effects of DAF-16 from the proximal somatic gonad that
491 act on the germ line should affect the DTC too, via feedback, since they preserve the PZ.
492 However, we did not observe the predicted stabilization of DTC processes when *daf-16(+)* was
493 expressed in the proximal somatic gonad in *daf-16(0); daf-2(rf)*. This result, together with the
494 more marked effect of muscle-expressed *daf-16* on the DTC versus the PZ suggest that the
495 germ cell interaction is not the sole arbiter of DTC stability with age. Finally, many aspects of the
496 germ cell cycle are unusual, including a highly abbreviated G1, constitutively high levels of
497 cyclin E/CDK2 throughout the cell cycle, and transcriptional regulation of CDK-2 through
498 inhibition of DPL-1 (Fox et al., 2011; Furuta et al., 2018). How such cell cycle features are
499 modified with age and how such modifications influence germ cell propensity to differentiate are
500 unresolved.
501
502 ***General implications for aging stem cell systems and regenerative medicine***
503 Our results demonstrate that niche morphology is a key aspect of aging stem cell
504 systems. Non-autonomous control of niche morphology, by tissues outside the stem cell system
505 and/or the adjacent stem cells, may be important in other stem cell systems as well. Our work
506 further suggests that deeper knowledge of *in vivo* interactions, especially those influenced by
507 cellular morphology and cell cycle as well as cell-cell signaling, are required to understand stem
508 cell behavior and tissue regeneration, especially in aging systems.
509
510
511 **MATERIALS AND METHODS**
512
513 ***Nematode strains and maintenance***
514 The *C. elegans* strains utilized in this study were raised on standard nematode growth media
515 (NGM) agar and *E. coli* OP50 at 20ºC, unless otherwise specified. All strains were derived from
516 Bristol N2 (Brenner, 1974). All strains, including their complete genotypes and sources, are
517 provided in Table S1. The strains generated in this study were obtained through genetic crosses
518 and homozygosity was confirmed by progeny testing – visually for strains bearing fluorescent

519 markers or by DNA sequence analysis based on information in WormBase (Davis et al., 2022).
520 Strains generated for this study are GC1593, GC1607, GC1616, GC1676, GC1682, GC1683,
521 GC1691, GC1692, GC1696, GC1748, GC1778, GC1817, GC1819, and GC1912, and are
522 available upon request.
523
524 ***Aging and lifespan assays***
525 Multiple plates of approximately 20 L4 hermaphrodites per plate were prepared, and worms
526 were transferred daily to fresh plates to prevent overcrowding and mixing with their progeny.
527 Worms were collected for imaging or PZ counting at intervals indicated. Controls were run in
528 parallel within each cohort; cohorts share a color in each figure that reports DTC morphometrics
529 or PZ nuclei counts, or mitotic index. Lifespan assays (Fig. 1A) started with 100 worms per
530 genotype. For N2 and CB1370, ~15% were censored due to bagging, desiccating on the petri
531 dish wall, or were otherwise missing. For the two strains that contain *qIs57* (JK2869 and
532 GC1607) the rate of censoring for the same reasons was higher, at 40-50%.
533
534 ***Imaging***
535 With the exception of images of GC1412 in Fig. S1, DTC images were acquired using a Apo
536 60X oil immersion lens on a Nikon W1 spinning disk confocal microscope and subsequently
537 processed, quantified, and analyzed as described in Gupta et al., 2024 (Gupta et al., 2024). The
538 DTC was visualized using the *qIs57* GFP marker, with a 488 nm excitation laser set at ≤10%
539 power. The exposure time was set to 100 ms or 1 frame, the EM Gain Multiplier was set to 50,
540 the conversion gain was set to 1, and the readout mode was set to 'EM Gain 10 MHz at 16-bit'.
541 The images were acquired as Z-stacks at 0.5 µm step size and saved in .nd2 format. The
542 excitation laser used for DAPI was 405 nm at 20-30% power, and for RFP was 561 nm at 20-
543 30% power range.
544
545 ***DAPI staining, progenitor zone (PZ) counts, and mitotic figures and index.***
546 DAPI staining (using Vectashield from Vector Laboratories™ H-1200-10) was performed as
547 described in Pepper et al., 2003, except that fixation and staining were done in a 9-well glass
548 depression plates (Corning™ 7220-85) to minimize the loss of older worms. Images were
549 acquired using a 60X oil immersion lens on a Nikon W1 spinning disk confocal microscope. The
550 progenitor zone (PZ) is defined as the region before the occurrence of more than one crescent-
551 shaped nucleus within the same transverse section of the gonad (Crittenden et al., 2006; Killian
552 and Hubbard, 2005). After visualizing the entire stack, the PZ region of interest was identified,

553 and the nuclei were counted manually using the multi-point tool in ImageJ™. Mitotic figures
554 were defined as obvious metaphase, anaphase, and early telophase figures as visualized in
555 images after whole-mount DAPI staining. Mitotic index is the number of mitotic figures over total
556 number of PZ nuclei.
557
558 ***Auxin-mediated degradation***
559 For auxin-inducible protein degradation (AID) experiments, 3 mM of Indole-3-acetic acid (IAA,
560 auxin) (Thermo Scientific™ A10556.14) or an equivalent volume of carrier EtOH for controls
561 was added to NGM agar prior to pouring plates. OP50 bacteria were concentrated
562 approximately 2x prior to seeding the auxin-containing plates to compensate for auxin inhibition
563 of bacterial growth (Zhang et al., 2022). Worms were cultured on both the auxin-containing
564 plates and the control plates for multiple generations prior to initiating the aging protocol.
565
566 ***Analysis of glp-1(e2141) and glp-4(bn2)***
567 Worms (*glp-1* and *glp-4* mutant with parallel controls) were collected at the mid-L4 stage and
568 cultured at 15°C for 48 and 72 hours, respectively, to allow for DTC elaboration comparable to
569 that seen in Day 1 adults raised at 20°C. For both genotypes, a group of worms were separated
570 from the cohort and imaged (T0). For *glp-1* experiments, the rest were shifted to 25°C and
571 imaged 24 and 48 hours later. For *glp-4* experiments, the rest were shifted to 25°C for 48 hours
572 and then shifted back to 15°C for another 48 hours. Cohorts of worms that were grown under
573 the same conditions were split and analyzed live for DTC features or for cell counts after DAPI
574 staining.
575
576 ***RNAi bacterial feeding***
577 RNAi feeding was carried out as previously described (Timmons et al., 2001) with minor
578 modifications. Single colonies of *E. coli* strain HT115 carrying either an empty vector (L4440) or
579 a vector containing *daf-16* cDNA sequences were obtained from frozen stocks on solid LB
580 plates supplemented with 100 µg/ml ampicillin and 10 µg/ml tetracycline, grown overnight at
581 37°C and used to inoculate liquid LB cultures supplemented with 100 µg/ml ampicillin. Cultures
582 were grown at 37°C with shaking for 6-8 hours and used to seed NGM plates supplemented
583 with 100 µg/ml ampicillin and 0.5% β-lactose. Seeded RNAi plates were kept at room
584 temperature for 24 hours prior to adding worms. Complete penetrance of the *bli-3* Bli phenotype
585 was used as a positive control to confirm the efficacy of RNAi reagents in each experimental
586 replicate. Fresh plates were seeded twice a week over the course of the experiment. L4

587 hermaphrodites were cultured on either L4440- or *daf-16* RNAi-seeded plates for 1 generation
588 prior to starting the aging assays.
589
590 ***Statistics***
591 Table S2 (.xlsx file) provides properties analyzed, means, SE/SD, and n values for all data
592 presented in main and supplementary figures (tab for each main and corresponding
593 supplemental figure). Table S3 (.xlsx file) lists the genotypes compared, statistical tests, and the
594 exact p values for each main and supplementary data figure on a separate tab. For lifespan
595 assays, the Mantel-Cox log-rank test was used. Fisher's exact test was used for pair-wise
596 comparisons of proportion plots (DTCs with nuclear displacement ≥5 μm, DTCs with any CPs
597 ≥20 μm, and PZs with mitotic figures at Day 10). For determining significance between nuclear
598 displacement, number, mean length, and maximum length of CPs ≥20 μm, the number of PZ
599 nuclei, or mitotic index: two-tailed t-test for pairwise comparisons (main figures), and two-tailed
600 t-test with Bonferroni correction for multiple comparisons (supplement). When reporting the
601 mean and maximum CP length, we did not include DTCs that with no CPs >20 μm. All sample
602 numbers (n) are also reported within figures.
603
604 **ACKNOWLEDGEMENTS**
605 We thank the CGC, which is funded by NIH Office of Research Infrastructure Programs (P40
606 OD010440), NYU Langone's Microscopy Laboratory (RRID: SCR_017934), especially Michael
607 Cammer; this shared resource is partially supported by the Cancer Center Support Grant
608 P30CA016087, Sophia Heimbrock for technical assistance, and Anke Kloock, Theadora Tolkin,
609 Julie Manikas and Caroline Goutte for advice and support.
610
611 **FUNDING**
612 NIH R01AG065672
613 NYSTEM DOH 01-C32560GG-3450000
614
615

616

617 **FIGURE LEGENDS**

618

619 **Figure 1. The age-related shift in DTC nuclear position and decline in DTC processes**
620 **number and length have different levels of dependence on *daf-2*.**
621 **(A)** Survival curves for *daf-2(+)* and *daf-2(rf)* worms with and without the *qIs57*[*lag-2p::GFP*]
622 transgene. N2 is the standard wild type, and age is indicated in days post mid-L4 stage.
623 **(B)** Representative micrographs of DTCs in live worms of the indicated genotypes at adult Day
624 1, 6 and 10, post mid-L4. The 20 µm region is between the dotted lines, and the area analyzed
625 for number and length of continuous processes (CPs; see Gupta et al., 2024; Tolkin et al., 2024)
626 is indicated between the dotted and dashed lines, the latter showing the position of the longest
627 CP. Arrows indicate the DTC nucleus. Open arrowheads indicate non-DTC structures. Scale
628 bars are 20 µm.
629 **(C)** Quantified age-related DTC features (from top left to bottom right): proportion of DTCs with
630 nuclear displacement ≥5 µm (black bar), position of nuclear displacement (µm) from the distal
631 end, proportion of DTCs with any CPs ≥20 µm (black bar), number of CPs ≥20 µm per DTC,
632 mean and maximum length of CPs ≥20 µm per DTC. N values for proportion plots are the same
633 as for the nuclear displacement superplot (top middle). For all superplots, each dot represents a
634 single DTC (n value shown), colors indicate parallel cohorts distinct from those in other main
635 figures, large circles in color are averages for each cohort, the black dot is the pooled average
636 for all cohorts shown, and black line connects pooled average values, indicating the direction
637 and extent of differences between Day 1 and Day 10. Day 10 n values for mean and maximum
638 CP length are lower since only DTCs with CPs >20 µm were included in these measurements.
639 **(D)** Number, mean and maximum length of CPs in *daf-2(rf)* at indicated ages in days post mid-
640 L4.
641 **For all panels**, *qIs57* carries *lag-2p::GFP* and *daf-2(rf)* is *daf-2(e1370).* See methods, Tables
642 S2, S3 for statistics details; comparisons are made between Day 1 and Day 10 within a given
643 genotype; for proportion plots, only $p < 0.05$ are indicated; otherwise, NS is "not significant", or p
644 ≥ 0.05; * $p < 0.05$; ** $p < 0.01$; *** $p < 0.001$.

645

646 **Figure 2. Loss of *daf-16* largely reverses the effects of *daf-2* on CP number and length.**
647 From top to bottom: proportion of DTCs with any CPs ≥20 µm (black bars), number of CPs ≥20
648 µm per DTC, mean and maximum length of CPs ≥20 µm per DTC in the indicated genotypes for
649 worms imaged on Day 1 and Day 10 post mid-L4. N values for proportion plots correspond to

650 the “Number of CPs” superplot to the right; n values for mean and maximum length plots reflect
651 only those DTCs with CPs ≥ 20 µm. For superplots, dots and circles are as described in Figure
652 1; colors indicate cohorts and replicates are distinct from those presented in other main figures.
653 See methods, Tables S2, S3 for statistics details; NS is “not significant”, * $p < 0.05$, ** $p < 0.01$,
654 *** $p < 0.001$, and blue asterisks indicate a significant increase from Day 1 to Day 10.
655
656
657 **Figure 3. *daf-16(+)* in body wall muscle is sufficient and necessary for *daf-2(rf)***
658 **suppression of age-related changes in DTC process length.**
659 **(A)** Proportion of DTCs with CPs ≥20 µm, and mean length of CPs ≥20 µm per DTC for
660 indicated genotypes (*daf-16(0); qIs57; daf-2(rf)* alone and with extrachromosomal arrays
661 expressing *daf-16a(+)*) at Day 1 and Day 10 post mid-L4. N values for mean length plots reflect
662 only those DTCs with CPs ≥ 20 µm. See Fig. S6 for additional timepoints and maximum length.
663 **(B)** Superplots showing mean length of CPs ≥20 µm in genotypes indicated. *L4440* indicates the
664 empty vector control and *daf-16 RNAi* is the vector carrying *daf-16* cDNA sequences. See Fig.
665 S8 for additional timepoints and maximum length. **(C)** Mean length of CPs ≥20 µm in worms
666 raised on 3mM auxin in genotypes indicated, where *daf-16::degron* is *hq389[daf-*
667 *16::GFP::degron]* and *Muscle::TIR1* is *emcSi71[myo-3p::TIR-1::mRuby]*. See Fig. S10 for
668 images, additional time points, and maximum length. **For all panels,** *qIs57* carries *lag-2p::GFP*,
669 *daf-16(0)* is *daf-16(mu86),* and *daf-2(rf)* is *daf-2(e1370).* For all superplots, colors indicate
670 cohorts within panels; replicates shown here are distinct from those in other main figures. See
671 methods, Tables S2, S3 for statistics details; NS is “not significant”, * $p < 0.05$, ** $p < 0.01$, *** p
672 < 0.001, and blue asterisks indicate a significant increase.
673
674 **Figure 4. Muscle-expressed *daf-16* influences both the rate of progenitor zone (PZ) pool**
675 **loss and continued germ cell divisions with age.**
676 **(A)** The number of PZ nuclei in (n) gonads in worms of the indicated genotypes at Day 1 and
677 Day 10 post mid-L4. **(B)** The proportion of PZs in Day 10 adults displaying one or more mitotic
678 figures. See Fig. S9C for mitotic index. See Table S3 for all pairwise comparisons. **For all**
679 **panels,** *qIs57* carries *lag-2p::GFP*, *daf-16(0)* is *daf-16(mu86),* and *daf-2(rf)* is *daf-2(e1370).* For
680 all superplots, colors indicate cohorts within panels. See methods, Tables S2, S3 for statistics
681 details; NS is “not significant”, *** $p < 0.001$.
682

683 **Figure 5. DTC processes decline prematurely with germline stem cell differentiation, but**
684 **not with restricted cell cycle progression.**
685 **(A, D)** Experimental design and images of DAPI-stained control and *glp-1(e2141ts)* (A) or *glp-*
686 *4(bn2ts)* (D) worms at 48 hours after shift to the restrictive temperature. White dotted lines
687 indicate the proximal border of the PZ. Asterisks indicate the distal end. **(B, E)** Examples of DTC
688 morphology in worms scored in parallel to those shown in panel (A)**.** Black dashed lines indicate
689 the longest CP. Arrows indicate the DTC nucleus. **(A,B,D,E)** Scale bars are 20 μm. **(C, F)**
690 Quantification of mean and maximum lengths of CPs ≥20 μm in control and *glp-1(e2141ts)* (C)
691 or *glp-4(bn2ts)* (F) worms at indicated time points. Colors indicate cohorts within panels. See
692 methods, Tables S2, S3 for statistics details; NS is "not significant", * $p < 0.05$, *** $p < 0.001$.
693
694 **Figure 6.** Cartoon representation of a two-component feedback model for niche-stem cell
695 interaction at early and late ("old") adult stages. Dotted box indicates area of direct DTC-
696 germline interaction that is lost with age. White circles represent undifferentiated germ cells, and
697 grey circles represent differentiated germ cells. See text for details.
698

REFERENCES

Austin, J. and Kimble, J. (1987). glp-1 is required in the germ line for regulation of the decision between mitosis and meiosis in C. elegans. *Cell* **51**, 589-599.

Beanan, M. J., & Strome, S. (1992). Characterization of a germ-line proliferation mutation in C. elegans. *Development (Cambridge, England)*, **116**, 755–766.

Brenner, S. (1974). The genetics of Caenorhabditis elegans. *Genetics* **77**, 71-94.

Brunet, A., Goodell, M. A. and Rando, T. A. (2023). Ageing and rejuvenation of tissue stem cells and their niches. *Nat Rev Mol Cell Biol* **24**, 45-62.

Byrd, D. T., Knobel, K., Affeldt, K., Crittenden, S. L. and Kimble, J. (2014). A DTC niche plexus surrounds the germline stem cell pool in Caenorhabditis elegans. *PLoS One* **9**, e88372.

Chavez, D. R., Snow, A. K., Smith, J. R., & Stanfield, G. M. (2018). Soma-germ line interactions and a role for muscle in the regulation of *C. elegans* sperm motility. *Development (Cambridge, England)*, **145**.

Crittenden, S. L., Leonhard, K. A., Byrd, D. T. and Kimble, J. (2006). Cellular analyses of the mitotic region in the Caenorhabditis elegans adult germ line. *Molecular biology of the cell* **17**, 3051-3061.

Davis, P., Zarowiecki, M., Arnaboldi, V., Becerra, A., Cain, S., Chan, J., Chen, W. J., Cho, J., da Veiga Beltrame, E., Diamantakis, S., et al. (2022). WormBase in 2022-data, processes, and tools for analyzing Caenorhabditis elegans. *Genetics* **220**.

Dillin, A., Crawford, D. K. and Kenyon, C. (2002). Timing requirements for insulin/IGF-1 signaling in C. elegans. *Science* **298**, 830-834.

DiLoreto, R. and Murphy, C. T. (2015). The cell biology of aging. *Mol Biol Cell* **26**, 4524-4531.

Fox, P. M. and Schedl, T. (2015). Analysis of Germline Stem Cell Differentiation Following Loss of GLP-1 Notch Activity in Caenorhabditis elegans. *Genetics* **201**, 167-184.

Fox, P. M., Vought, V. E., Hanazawa, M., Lee, M.-H., Maine, E. M. and Schedl, T. (2011). Cyclin E and CDK-2 regulate proliferative cell fate and cell cycle progression in the C. elegans germline. *Development (Cambridge, England)* **138**, 2223-2234.

Furuta, T., Joo, H. J., Trimmer, K. A., Chen, S. Y. and Arur, S. (2018). GSK-3 promotes S-phase entry and progression in C. elegans germline stem cells to maintain tissue output. *Development* **145**.

Garigan, D., Hsu, A. L., Fraser, A. G., Kamath, R. S., Ahringer, J. and Kenyon, C. (2002). Genetic analysis of tissue aging in Caenorhabditis elegans: a role for heat-shock factor and bacterial proliferation. *Genetics* **161**, 1101-1112.

Gordon, K. L., Payne, S. G., Linden-High, L. M., Pani, A. M., Goldstein, B., Hubbard, E. J. A., & Sherwood, D. R. (2019). Ectopic Germ Cells Can Induce Niche-like Enwrapment by Neighboring Body Wall Muscle. *Current biology : CB*, **29**, 823–833.e5.

Gupta, N., Cammer, M., Tolkin, T. and Hubbard, E. J. A. (2024). A DTC morphometrics package for quantification of complex and variable cellular morphology using ImageJ. *MicroPubl Biol* **2024**.

Hall, D. H., Winfrey, V. P., Blaeuer, G., Hoffman, L. H., Furuta, T., Rose, K. L., Hobert, O. and Greenstein, D. (1999). Ultrastructural features of the adult hermaphrodite gonad of Caenorhabditis elegans: relations between the germ line and soma. *Dev Biol* **212**, 101-123.

Henderson, S. T., Gao, D., Lambie, E. J. and Kimble, J. (1994). lag-2 may encode a signaling ligand for the GLP-1 and LIN-12 receptors of C. elegans. *Development (Cambridge, England)* **120**, 2913-2924.

Herndon, L. A., Schmeissner, P. J., Dudaronek, J. M., Brown, P. A., Listner, K. M., Sakano, Y., Paupard, M. C., Hall, D. H. and Driscoll, M. (2002). Stochastic and genetic factors influence tissue-specific decline in ageing C. elegans. *Nature* **419**, 808-814.

Kenyon, C. (2010a). The first long-lived mutants: discovery of the insulin/IGF-1 pathway for ageing. *Philosophical Transactions of the Royal Society B: Biological Sciences* **366**, 9-16.

Kenyon, C., Chang, J., Gensch, E., Rudner, A. and Tabtiang, R. (1993). A C. elegans mutant that lives twice as long as wild type. *Nature* **366**, 461-464.

Kenyon, C. J. (2010b). The genetics of ageing. *Nature* **464**, 504-512.

Kershner, A., Crittenden, S. L., Friend, K., Sorensen, E. B., Porter, D. F. and Kimble, J. (2013). Germline Stem Cells and Their Regulation in the Nematode Caenorhabditis elegans. pp. 29-46. Dordrecht: Springer Netherlands.

Killian, D. J. and Hubbard, E. J. A. (2005). Caenorhabditis elegans germline patterning requires coordinated development of the somatic gonadal sheath and the germ line. *Developmental Biology* **279**, 322-335.

Kimble, J. E. and White, J. G. (1981). On the control of germ cell development in Caenorhabditis elegans. *Dev Biol* **81**, 208-219.

Kimura, K. D., Tissenbaum, H. A., Liu, Y. and Ruvkun, G. (1997). daf-2, an insulin receptor-like gene that regulates longevity and diapause in Caenorhabditis elegans. *Science* **277**, 942-946.

Kocsisova, Z., Bagatelas, E. D., Santiago-Borges, J., Lei, H. C., Egan, B. M., Mosley, M. C., Anderson, A. M., Schneider, D. L., Schedl, T., & Kornfeld, K. (2025). Notch signaling in germ line stem cells controls reproductive aging in *Caenorhabditis elegans*. *PNAS nexus*, **4**.

Kocsisova, Z., Kornfeld, K. and Schedl, T. (2019). Rapid population-wide declines in stem cell number and activity during reproductive aging in C. elegans. *Development* **146**.

Kumsta, C. and Hansen, M. (2012). C. elegans rrf-1 mutations maintain RNAi efficiency in the soma in addition to the germline. *PLoS One* **7**, e35428.

Lee, C., Sorensen, E. B., Lynch, T. R. and Kimble, J. (2016). C. elegans GLP-1/Notch activates transcription in a probability gradient across the germline stem cell pool. *eLife* **5**.

Libina, N., Berman, J. R. and Kenyon, C. (2003). Tissue-specific activities of C. elegans DAF-16 in the regulation of lifespan. *Cell* **115**, 489-502.

Lopez-Otin, C., Blasco, M. A., Partridge, L., Serrano, M. and Kroemer, G. (2023). Hallmarks of aging: An expanding universe. *Cell* **186**, 243-278.

Luo, S., Kleemann, G. A., Ashraf, J. M., Shaw, W. M. and Murphy, C. T. (2010). TGF-β and insulin signaling regulate reproductive aging via oocyte and germline quality maintenance. *Cell* **143**, 299-312.

Michaelson, D., Korta, D. Z., Capua, Y. and Hubbard, E. J. A. (2010). Insulin signaling promotes germline proliferation in C. elegans. *Development (Cambridge, England)* **137**, 671-680.

Mok, D. Z., Sternberg, P. W. and Inoue, T. (2015). Morphologically defined sub-stages of C. elegans vulval development in the fourth larval stage. *BMC Dev Biol* **15**, 26.

Murphy, C. T. and Hu, P. J. (2013). Insulin/insulin-like growth factor signaling in C. elegans. *WormBook*, 1-43.

Nadarajan, S., Govindan, J. A., McGovern, M., Hubbard, E. J. A. and Greenstein, D. (2009). MSP and GLP-1/Notch signaling coordinately regulate actomyosin-dependent cytoplasmic streaming and oocyte growth in C. elegans. *Development (Cambridge, England)* **136**, 2223-2234.

Qin, Z. and Hubbard, E. J. A. (2015). Non-autonomous DAF-16/FOXO activity antagonizes age-related loss of C. elegans germline stem/progenitor cells. *Nature Communications* **6**, 7107.

Roy, D., Michaelson, D., Hochman, T., Santella, A., Bao, Z., Goldberg, J. D. and Hubbard, E. J. A. (2016). Cell cycle features of C. elegans germline stem/progenitor cells vary temporally and spatially. *Dev Biol* **409**, 261-271.

Russell, S. J. and Kahn, C. R. (2007). Endocrine regulation of ageing. *Nat Rev Mol Cell Biol* **8**, 681-691.

Sabatella, M., Thijssen, K. L., Davo-Martinez, C., Vermeulen, W. and Lans, H. (2021). Tissue-Specific DNA Repair Activity of ERCC-1/XPF-1. *Cell Rep* **34**, 108608.

Siegfried, K. R., Kidd, A. R., 3rd, Chesney, M. A. and Kimble, J. (2004). The sys-1 and sys-3 genes cooperate with Wnt signaling to establish the proximal-distal axis of the Caenorhabditis elegans gonad. *Genetics* **166**, 171-186.

Sijen, T., Fleenor, J., Simmer, F., Thijssen, K. L., Parrish, S., Timmons, L., Plasterk, R. H. and Fire, A. (2001). On the role of RNA amplification in dsRNA-triggered gene silencing. *Cell* **107**, 465-476.

Timmons, L., Court, D. L. and Fire, A. (2001). Ingestion of bacterially expressed dsRNAs can produce specific and potent genetic interference in Caenorhabditis elegans. *Gene* **263**, 103-112.

Tolkin, T., Burnett, J. and Hubbard, E. J. A. (2024). A role for organ level dynamics in morphogenesis of the C. elegans hermaphrodite distal tip cell. *Development* **151**.

Uno, M., Tani, Y., Nono, M., Okabe, E., Kishimoto, S., Takahashi, C., Abe, R., Kurihara, T. and Nishida, E. (2021). Neuronal DAF-16-to-intestinal DAF-16 communication underlies organismal lifespan extension in C. elegans. *iScience* **24**, 102706.

Urman, M. A., John, N. S., Jung, T. and Lee, C. (2024). Aging disrupts spatiotemporal regulation of germline stem cells and niche integrity. *Biol Open* **13**.

Vogel, B. E., & Hedgecock, E. M. (2001). Hemicentin, a conserved extracellular member of the immunoglobulin superfamily, organizes epithelial and other cell attachments into oriented line-shaped junctions. *Development (Cambridge, England)*, **128**, 883–894.

Wang, H., Webster, P., Chen, L. and Fisher, A. L. (2019). Cell-autonomous and non-autonomous roles of daf-16 in muscle function and mitochondrial capacity in aging C. elegans. *Aging (Albany NY)* **11**, 2295-2311.

Zhang, L., Ward, J. D., Cheng, Z. and Dernburg, A. F. (2015). The auxin-inducible degradation (AID) system enables versatile conditional protein depletion in C. elegans. *Development* **142**, 4374-4384.

Zhang, Y. P., Zhang, W. H., Zhang, P., Li, Q., Sun, Y., Wang, J. W., Zhang, S. O., Cai, T., Zhan, C. and Dong, M. Q. (2022). Intestine-specific removal of DAF-2 nearly doubles lifespan in Caenorhabditis elegans with little fitness cost. *Nat Commun* **13**, 6339.

Zhang, Z., Yang, H., Fang, L., Zhao, G., Xiang, J., Zheng, J. C. and Qin, Z. (2024). DOS-3 mediates cell-non-autonomous DAF-16/FOXO activity in antagonizing age-related loss of C. elegans germline stem/progenitor cells. *Nat Commun* **15**, 4904.

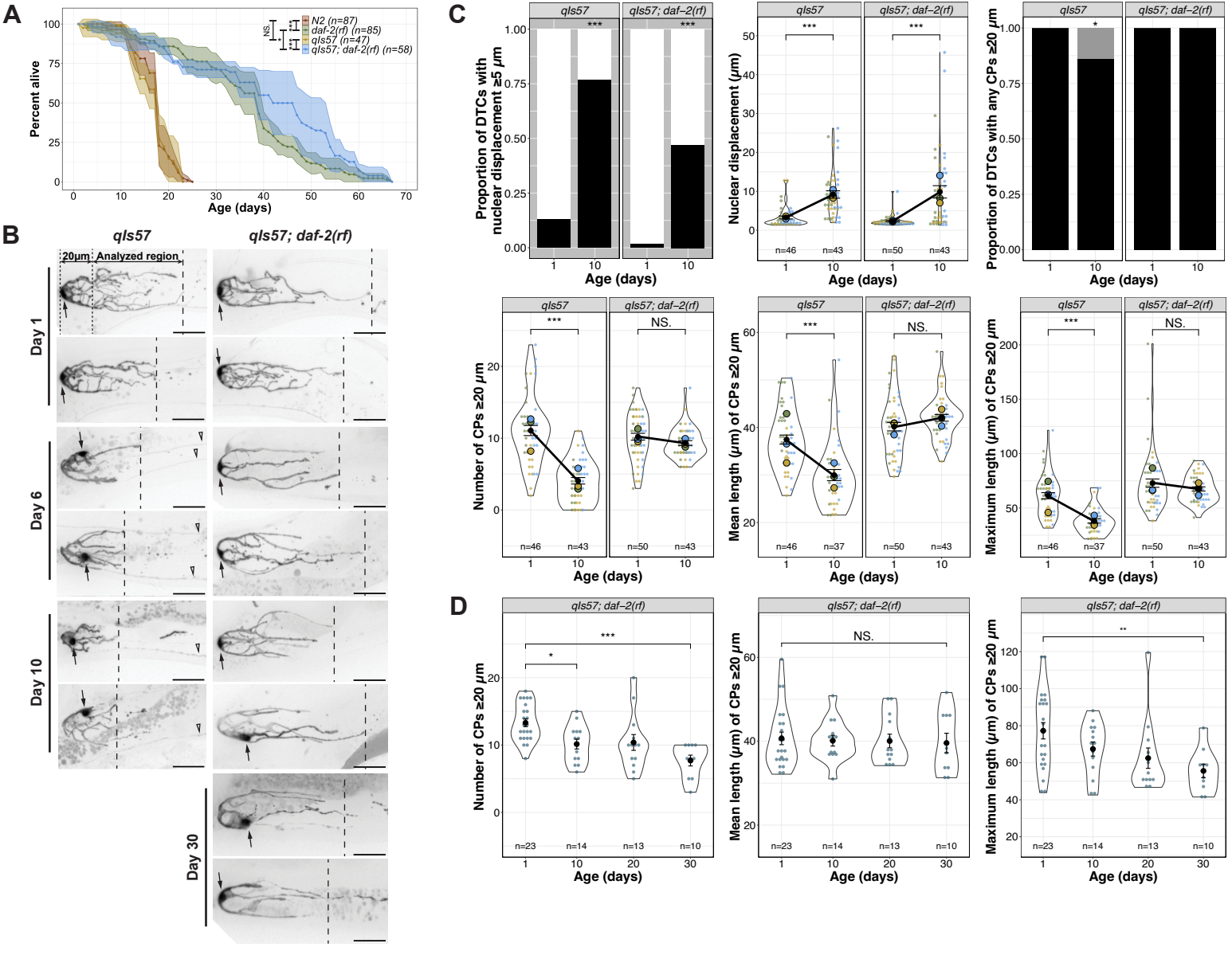
A
Percent alive
Age (days)
N2 (n=87)
daf-2(rf) (n=85)
qls57 (n=47)
qls57; daf-2(rf) (n=58)
NS.
***
B
qls57
qls57; daf-2(rf)
20µm
Analyzed region
Day 1
Day 6
Day 10
Day 30
C
qls57
qls57; daf-2(rf)
Proportion of DTCs with nuclear displacement ≥5 µm
Nuclear displacement (µm)
Proportion of DTCs with any CPs ≥20 µm
Number of CPs ≥20 µm
Mean length (µm) of CPs ≥20 µm
Maximum length (µm) of CPs ≥20 µm
Age (days)
n=46
n=43
n=50
n=43
n=37
D
n=23
n=14
n=13
n=10

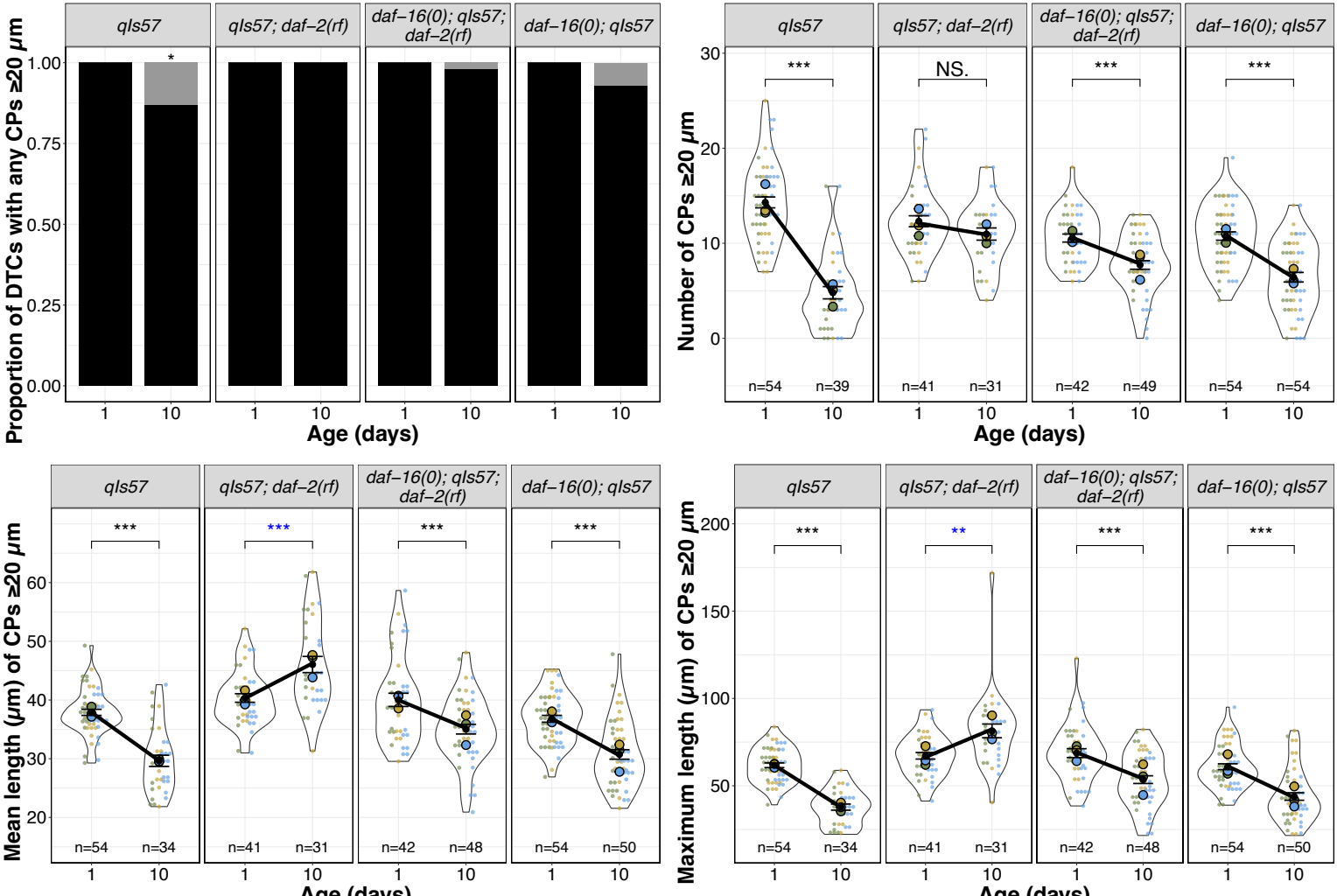
qls57
qls57; daf−2(rf)
daf−16(0); qls57; daf−2(rf)
daf−16(0); qls57
Proportion of DTCs with any CPs ≥20 μm
1.00
0.75
0.50
0.25
0.00
*
Number of CPs ≥20 μm
30
20
10
0
***
NS.
n=54
n=39
n=41
n=31
n=42
n=49
Mean length (μm) of CPs ≥20 μm
60
50
40
30
20
n=34
n=48
n=50
Maximum length (μm) of CPs ≥20 μm
200
150
100
50
**
1
10
Age (days)

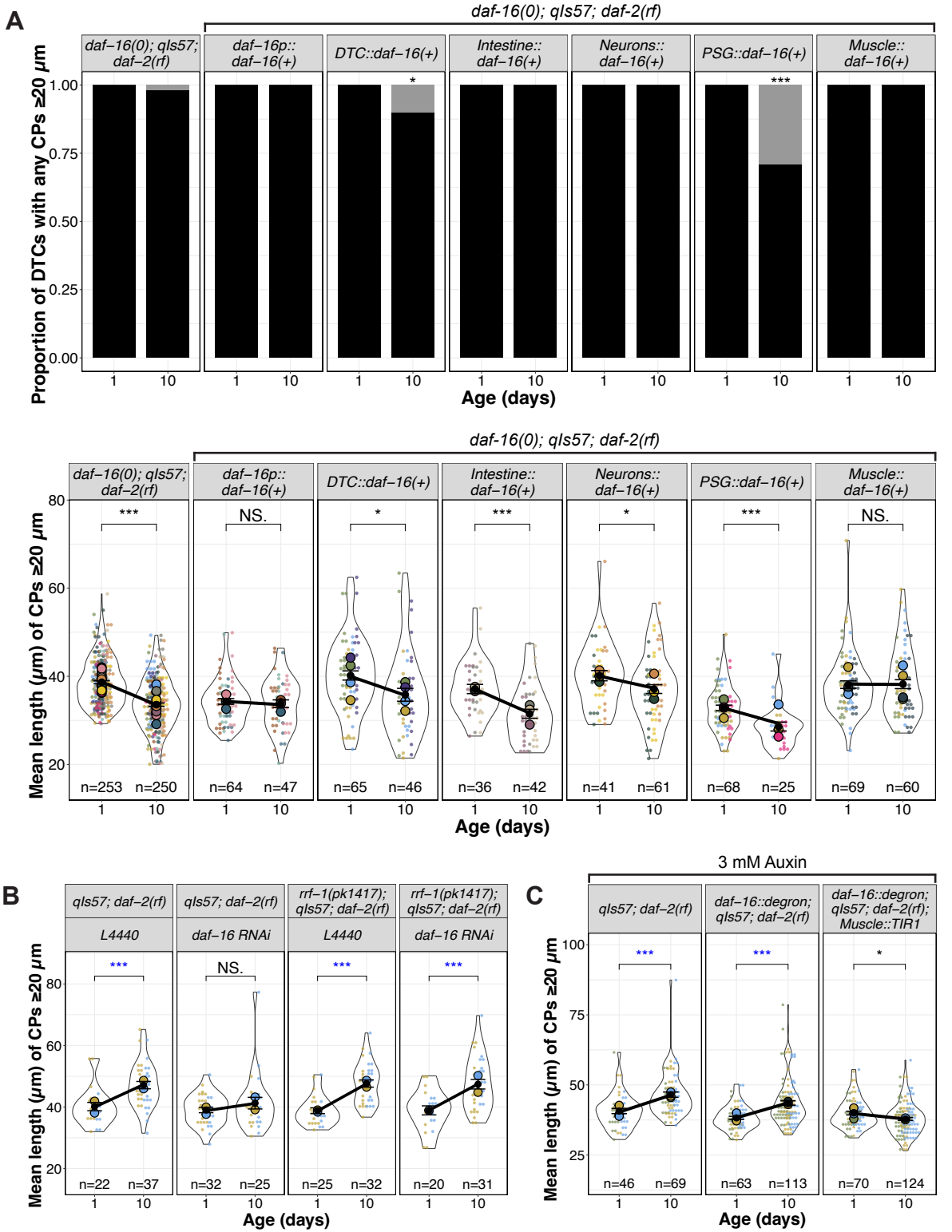
A
daf-16(0); qIs57; daf-2(rf)
daf−16(0); qIs57; daf−2(rf)
daf−16p:: daf−16(+)
DTC::daf−16(+)
Intestine:: daf−16(+)
Neurons:: daf−16(+)
PSG::daf−16(+)
Muscle:: daf−16(+)
Proportion of DTCs with any CPs ≥20 μm
1.00
0.75
0.50
0.25
0.00
*
***
1
10
Age (days)
Mean length (μm) of CPs ≥20 μm
80
60
40
20
***
NS.
*
***
*
***
NS.
n=253
n=250
n=64
n=47
n=65
n=46
n=36
n=42
n=41
n=61
n=68
n=25
n=69
n=60
B
qIs57; daf−2(rf)
L4440
qIs57; daf−2(rf)
daf−16 RNAi
rrf−1(pk1417); qIs57; daf−2(rf)
L4440
rrf−1(pk1417); qIs57; daf−2(rf)
daf−16 RNAi
n=22
n=37
n=32
n=25
n=25
n=32
n=20
n=31
C
3 mM Auxin
qIs57; daf−2(rf)
daf−16::degron; qIs57; daf−2(rf)
daf−16::degron; qIs57; daf−2(rf); Muscle::TIR1
100
75
50
25
n=46
n=69
n=63
n=113
n=70
n=124

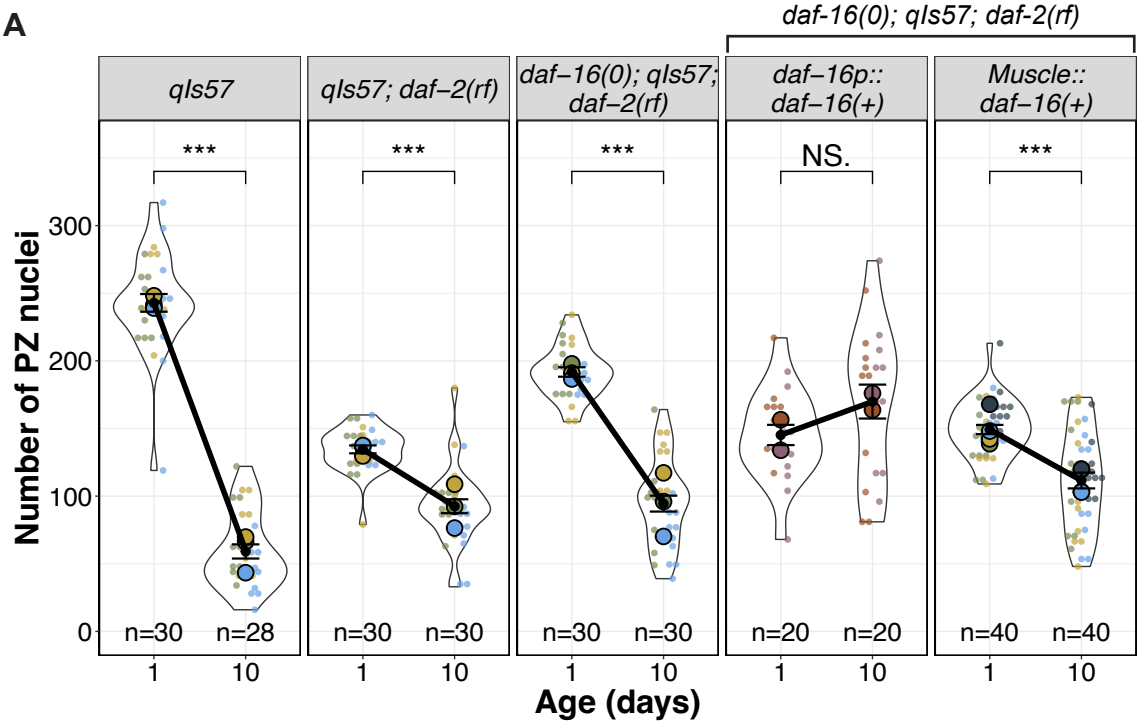
A
daf-16(0); qIs57; daf-2(rf)
qIs57
qIs57; daf–2(rf)
daf–16(0); qIs57; daf–2(rf)
daf–16p:: daf–16(+)
Muscle:: daf–16(+)
***
***
***
NS.
***
Number of PZ nuclei
300
200
100
0
n=30
n=28
n=30
n=30
n=30
n=30
n=20
n=20
n=40
n=40
1
10
Age (days)

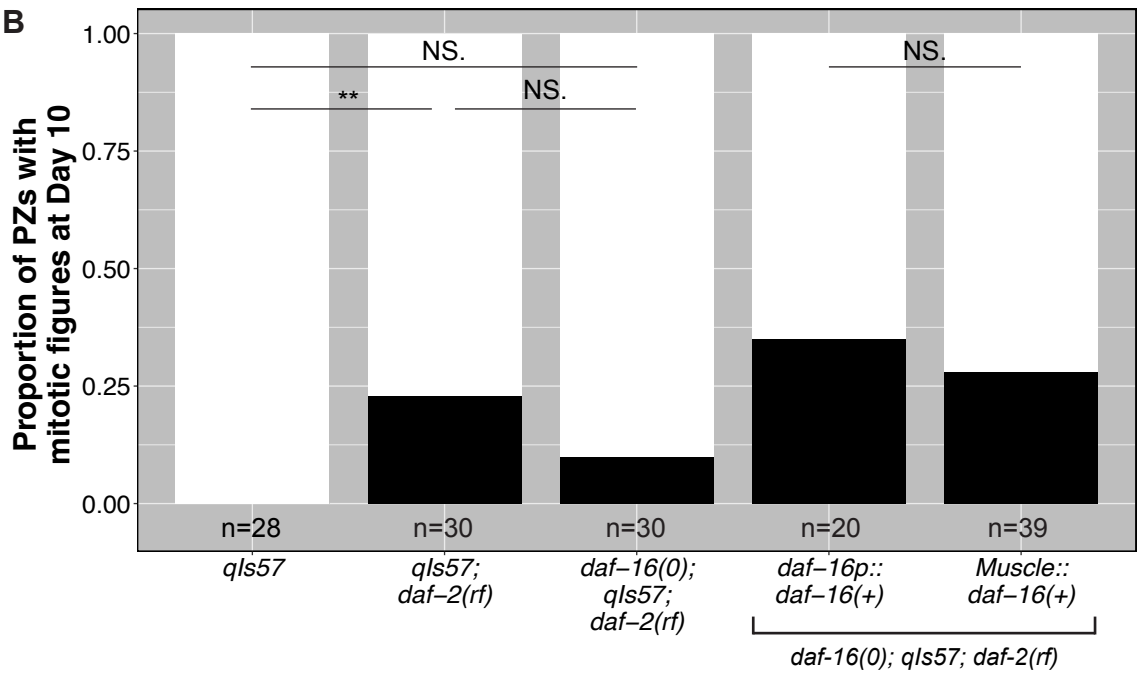
B
Proportion of PZs with mitotic figures at Day 10
1.00
0.75
0.50
0.25
0.00
NS.
**
NS.
NS.
n=28
n=30
n=30
n=20
n=39
qIs57
qIs57; daf–2(rf)
daf–16(0); qIs57; daf–2(rf)
daf–16p:: daf–16(+)
Muscle:: daf–16(+)
daf-16(0); qIs57; daf-2(rf)

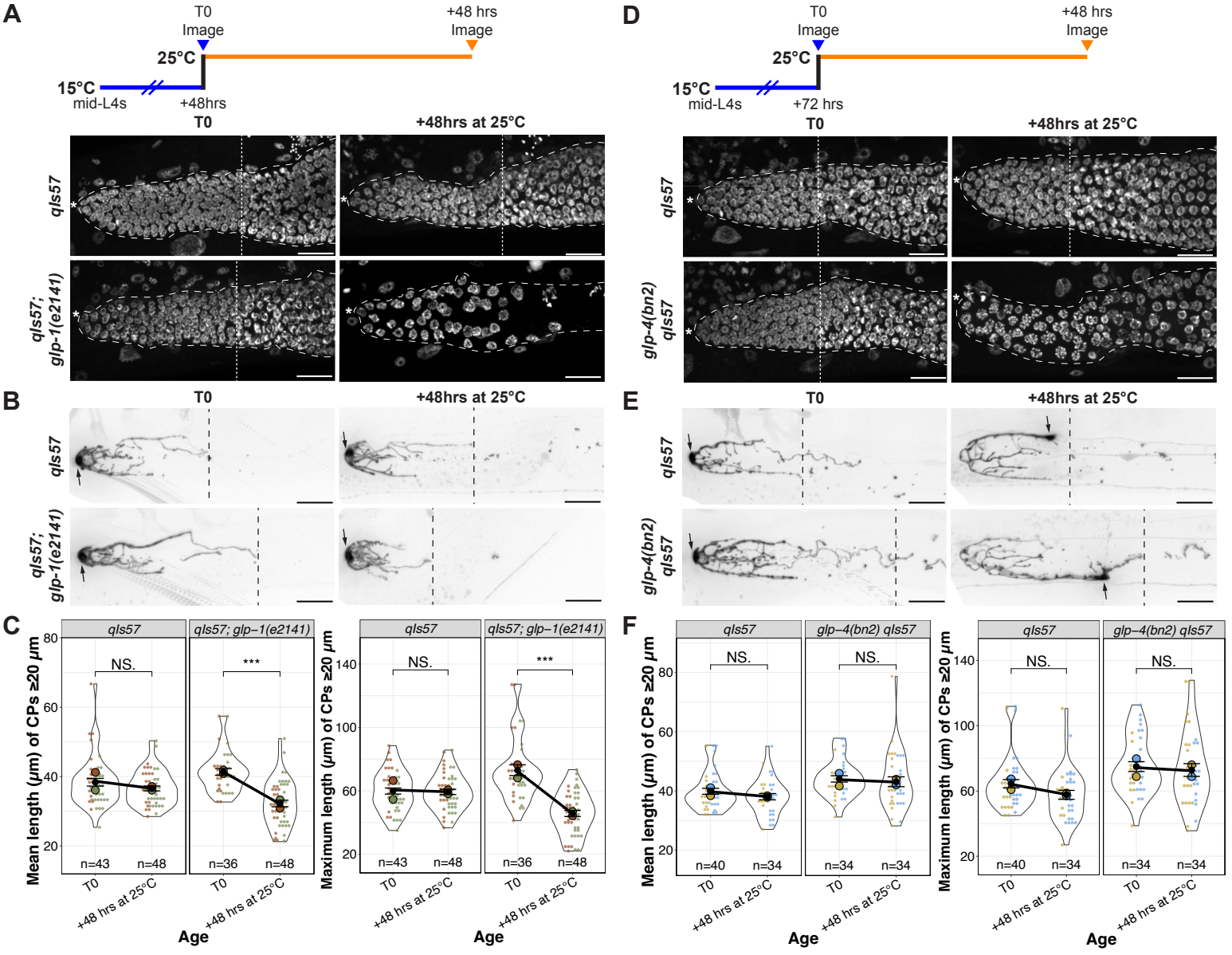
A
T0
Image
+48 hrs
Image
25°C
15°C
mid-L4s
+48hrs
T0
+48hrs at 25°C
qIs57
qIs57;
glp-1(e2141)
B
T0
+48hrs at 25°C
qIs57
qIs57;
glp-1(e2141)
C
qIs57
qIs57; glp−1(e2141)
NS.
***
Mean length (μm) of CPs ≥20 μm
Maximum length (μm) of CPs ≥20 μm
n=43
n=48
n=36
n=48
T0
+48 hrs at 25°C
Age
D
T0
Image
+48 hrs
Image
25°C
15°C
mid-L4s
+72 hrs
T0
+48hrs at 25°C
qIs57
glp-4(bn2)
qIs57
E
T0
+48hrs at 25°C
qIs57
glp-4(bn2)
qIs57
F
qIs57
glp−4(bn2) qIs57
NS.
Mean length (μm) of CPs ≥20 μm
Maximum length (μm) of CPs ≥20 μm
n=40
n=34
n=34
n=34
T0
+48 hrs at 25°C
Age

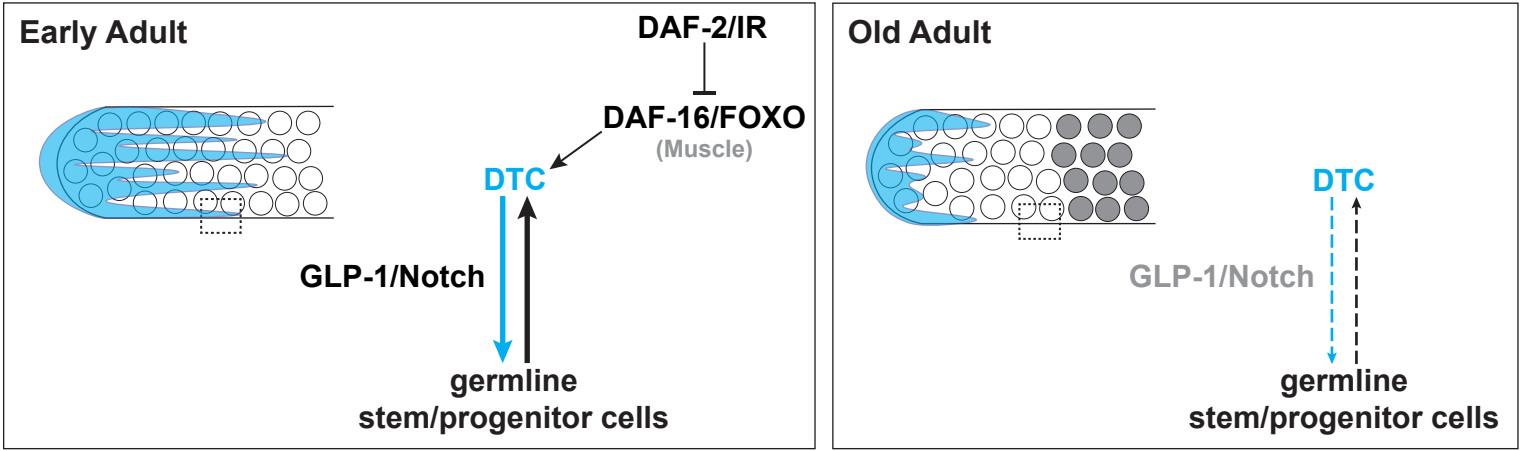
Early Adult
DAF-2/IR
DAF-16/FOXO
(Muscle)
DTC
GLP-1/Notch
germline
stem/progenitor cells
Old Adult
DTC
GLP-1/Notch
germline
stem/progenitor cells